Applied Physics Letters

RESEARCH ARTICLE | FEBRUARY 06 2025

Efficient room-temperature spin-amplified luminescence of an InAs quantum dot tunnel coupled with a thin GaNAs spin filter

Satoshi Hiura ; Shino Sato; Shunsuke Sakano ; Junichi Takayama ; Akihiro Murayama

Appl. Phys. Lett. 126, 052403 (2025)
https://doi.org/10.1063/5.0249606

Applied Physics Letters ARTICLE pubs.aip.org/aip/apl

Efficient room-temperature spin-amplified luminescence of an InAs quantum dot tunnel coupled with a thin GaNAs spin filter

Cite as: Appl. Phys. Lett. **126**, 052403 (2025); doi: 10.1063/5.0249606
Submitted: 19 November 2024 · Accepted: 28 January 2025 ·
Published Online: 6 February 2025

Satoshi Hiura,[a] Shino Sato, Shunsuke Sakano, Junichi Takayama, and Akihiro Murayama

AFFILIATIONS

Faculty of Information Science and Technology, Hokkaido University, Sapporo 060-0814, Japan

[a]Author to whom correspondence should be addressed: hiura@ist.hokudai.ac.jp

ABSTRACT

Dilute nitride GaNAs has attracted much attention for spin generation owing to its defect-engineered spin filtering at room temperature. Strong, circularly polarized luminescence reflecting the spin-polarized electron states generated by a GaNAs spin filter is needed to realize practical opto-spintronics applications. This study examined the impacts of the GaNAs thickness on the room-temperature spin-polarized luminescence properties of tunnel-coupled InAs quantum dots (QDs) through polarization- and time-resolved photoluminescence in combination with a rate equation analysis. Reducing the GaNAs thickness from 20 to 5 nm increased the QD luminescence intensity by over an order of magnitude at low excitation powers. This increased luminescence was attributed to decreased electron capture in the deep-level defect states of GaNAs, which resulted from fewer defects in thinner GaNAs layers. Furthermore, the reduction in GaNAs thickness decreased the excitation power needed to maximize electron spin polarization of QDs while maintaining a near-maximum value. This efficient spin-amplified luminescence of QDs was achieved through spin-selective capture of QD electrons by defect states under low excitation spin densities. These results demonstrate that using a thin GaNAs spin filter can result in strong QD luminescence and high circular polarization at room temperature and low excitation spin densities. The findings give valuable implications for the development of spin-functional optical devices utilizing a GaNAs spin filter.

The development of a spin-based information technology platform is essential for the realization of energy-saving information systems.[1–3] Magnetic random-access memory, which utilizes electron spins as information carriers, shows great promise as a replacement for charge-based dynamic random-access memory.[4] This spin-based nonvolatile memory can reduce power consumption by eliminating standby power.[5,6] Optical wiring can solve problems associated with conventional electrical wiring for short-range information communication. Optical wiring offers advantages, such as no thermal loss of energy, low signal delay, and large bandwidth. Therefore, the optical transfer of electron spin information is crucial in connecting spintronics-based memory and optical communication systems. III-V semiconductors can convert spin-polarized electron states into circularly polarized light through the optical-transition selection rule.[7] In (Ga)As quantum dots (QDs) serve as excellent spin–photon interfaces owing to their high luminescence efficiency[8,9] and ability to suppress spin relaxation.[10–12] However, at room temperature (RT), the spin polarization of electrons is rapidly reduced during injection from the GaAs barrier into QDs and upon reinjection into QDs after escaping.[13,14] This loss of spin polarization degrades the efficiency of spin-photon conversion using QDs. Therefore, the injection of highly spin-polarized electrons into QDs at RT is necessary to enhance the spin-polarized QD luminescence properties.

Dilute nitride GaNAs have emerged as promising candidates for spin generation. Deep-level defect states (DSs) derived from Ga^{2+} interstitials can enhance the spin polarization of the conduction-band electrons at RT through spin-dependent recombination.[15,16] First, the residual electrons in the Ga^{2+} paramagnetic defects are unpolarized, When spin-polarized electrons are injected into the conduction band, they become trapped in the DSs. Owing to the equal probability of recombination between spin-up and spin-down defect electrons with holes, a cycle of electron spin capture and recombination creates a spin imbalance of the defect electrons. The spin-polarized defects activate the spin filtering by capturing the conduction-band electrons with the opposite spin direction. Consequently, the spin polarization of conduction-band electrons is amplified. Recent advancements

demonstrated the achievement of electron spin polarization above 90% at RT by utilizing a tunnel-coupled nanostructure comprising a 20-nm-thick GaNAs quantum well (QW) and InAs QDs.[17] This structure allows for the injection of spin-amplified electrons from GaNAs to QDs, as well as the selective transfer of minority spins from QDs to DSs through QW-QD wavefunction coupling.[18,19] However, the proximity of GaNAs spin filter to QDs reduces QD luminescence intensity owing to electron capture in the DSs. Strong, circularly polarized luminescence reflecting the spin-polarized electron states generated by GaNAs is essential for opto-spintronics applications. In this study, the effects of GaNAs thickness on the circularly polarized QD luminescence properties were investigated through time- and polarization-resolved photoluminescence (PL) in combination with a rate equation analysis. When the GaNAs thickness was reduced from 20 to 5 nm, strong luminescence and high electron spin polarization of the QDs were achieved at RT under low excitation spin densities.

The samples investigated in this study were prepared using a molecular beam epitaxy equipped with a radio frequency plasma source for nitrogen [Fig. 1(a)]. After the growth of the GaAs buffer on the semi-insulating GaAs(100) substrate, a dilute nitride GaNAs layer with a thickness d was grown. The nitrogen content was adjusted to approximately 1% by controlling the radio frequency power and N_2 flow rate. Subsequently, the 3.8-ML-thick InAs QDs were formed after the growth of a 3-nm-thick GaAs tunneling barrier and capped with GaAs. An additional QD layer was formed on the surface for structural observation. In this study, four samples with $d = 5$, 10, 15, and 20 nm were prepared. Additionally, an InAs QD sample without GaNAs ($d = 0$ nm) was also prepared for comparison. The other growth conditions can be found elsewhere.[19,20]

Time- and polarization-resolved PL experiments were conducted at RT under σ^+-polarized excitation using a mode-locked Ti:Sapphire pulsed laser with a repetition rate of 80 MHz and a pulse width of <100 fs. The excitation power was changed from 0.5 to 50 mW, with a laser spot size estimated at 50 μm and a full-width half maximum of the laser pulse time response curve at approximately 4 ps. The laser wavelength was set to 850 nm to generate spin-polarized carriers in GaAs, with an expected electron spin polarization of 50% based on the optical-transition selection rule.[7] Although an 850 nm wavelength laser can excite carriers in GaNAs, the carrier excitation in GaNAs cannot contribute to the QD PL properties because of the sufficiently small volume ratio of the GaNAs layer to the GaAs layer. The PL circular polarization degree (CPD) is defined as $(I_{\sigma^+} - I_{\sigma^-})/(I_{\sigma^+} + I_{\sigma^-})$ using the circularly polarized PL intensity $I_{\sigma^\pm}$, reflecting the electron spin polarization at QD states.[17] Details of the optical orientation experiments are outlined elsewhere.[18]

Atomic force microscopy (AFM) images of surface QDs and their size distributions are shown in Figs. 1(b) and 1(c), respectively. The observation revealed an areal QD density of 3.2×10^{10} cm^{-2}. The QD

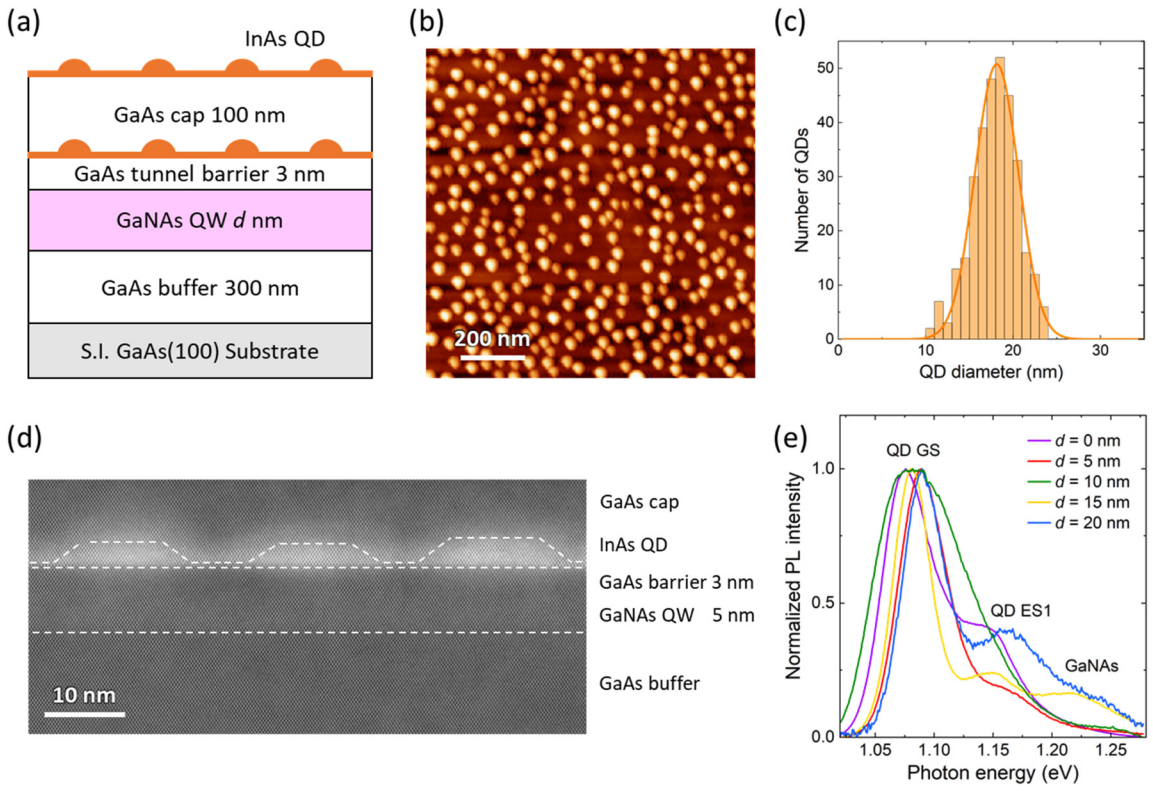

FIG. 1. (a) Schematic of the GaNAs QW-InAs QD tunnel-coupled sample structure. (b) AFM image of surface InAs QDs. (c) Size distribution of surface QDs with a Gaussian distribution curve (orange solid line). (d) HAADF-STEM image of GaNAs QW-InAs QD tunnel-coupled structure with a GaNAs thickness of 5 nm. (e) Normalized RT PL spectra measured with an excitation power of 3 mW.

ensembles were characterized by a symmetric size distribution with a mean diameter of 18 nm and a standard deviation of 2.6 nm. The radius of curvature of the AFM tip was considered for estimating the QD diameter.[18] The AFM analyses validated the formation of uniform QD ensembles. A high-angle annular dark-field scanning transmission electron microscopy (HAADF-STEM) image of the GaNAs QW-InAs QD tunnel-coupled structure with $d = 5$ nm is shown in Fig. 1(d). The QD base lengths and heights ranged from 17 to 20 and 3 to 4 nm, respectively. These base lengths were similar to the diameters of the surface QDs obtained using AFM, indicating that the presence of GaNAs has minimal impact on subsequent QD growth. This interpretation was supported by the normalized RT PL spectra [Fig. 1(e)]. The PL emission primarily originated from the QD ground state (GS) and first excited state (ES1). No significant difference in the QD GS was observed, indicating identical QD growth regardless of the GaNAs thickness. Small PL peaks and shoulders arising from the GaNAs QW were observed at 1.23–1.24 eV. The broad PL spectrum reflecting the non-uniform QD size distribution for $d = 10$ nm sample can be due to time-varying conditions, such as growth rate and arsenic pressure.

The PL spectra of the QDs measured at an excitation power of 5 mW are shown in Fig. 2(a). The PL intensity increased significantly with a decrease in d. Specifically, for the QD GS, the peak PL intensity increased by over fourfold, fourfold, and 18-fold for $d = 15$, 10, and 5 nm samples, respectively, compared with the $d = 20$ nm sample. Conversely, the PL intensity of the sample with $d = 20$ nm decreased by two orders of magnitude compared with the sample with $d = 0$ nm, whereas the decrease in PL intensity was significantly suppressed for the sample with $d = 5$ nm, being only approximately 1/3. This result highlights the effectiveness of reducing the GaNAs thickness in enhancing the QD PL intensity. The strong PL observed can be attributed to the reduced electron capture by the GaNAs DSs, which originated from their smaller numbers. The integrated PL intensity of the QD GS and corresponding PL intensity ratio between $d = 5$, 10, 15, and 20 nm samples and $d = 0$ nm sample as functions of the excitation power are shown in Figs. 2(b) and 2(c), respectively. The analyzed energy range was defined as 1.07–1.11 eV. The PL intensity ratio increased with increasing excitation power, reaching saturation at high excitation powers. For the GaNAs-QD samples, the photoexcited electrons were easily captured in the DSs at low excitation powers. The dominant electron capture accounts for the large PL intensity difference compared with that of the $d = 0$ nm sample. However, as the excitation power increased, the DSs became occupied, suppressing electron capture and allowing more electrons to be injected into the QDs. Notably, the PL intensity ratio was saturated at higher excitation powers for samples with thicker GaNAs. This feature was also evident from the integrated PL intensity [Fig. 2(b)]. As the number of DSs increases with the thickness of the GaNAs, a higher excitation power is required to occupy the DSs. These findings highlight the potential for achieving strong QD PL under low carrier density by reducing the thickness of GaNAs. However, the QD PL intensity remained unchanged when the GaNAs thickness was reduced from 15 to 10 nm. This result can be attributed to the QD quality, and the strongest wavefunction coupling between the GaNAs QW and QD, as reported in a previous study.[19] In this case, the transfer of electrons from QDs to DSs through wavefunction coupling may be promoted.

Furthermore, the CPD properties of QD PL were examined. The circularly polarized PL and CPD spectra of $d = 5$ and 20 nm samples are shown in Figs. 3(a) and 3(b), respectively. The excitation powers were set to 5 and 50 mW for $d = 5$ and 20 nm samples, respectively. Notably, the CPD values for the QD GS were identical at 40%–45% with similar PL intensity,indicating the potential for achieving high spin polarization of QDs at lower excitation powers through the reduction of GaNAs thickness. The excitation power dependence of the PL CPD is shown in Fig. 3(c). The CPD of the $d = 0$ nm sample decreased with excitation power owing to the state-filling effect in the QDs.[20–24] In contrast, significant CPD increases were observed in the GaNAs-QD samples with excitation power. The power-dependent CPD properties suggest the presence of power-dependent spin filtering in GaNAs.[25] Although similar CPD values of 14%–19% were observed at 0.5 mW, the CPD increases were steeper for samples with thinner

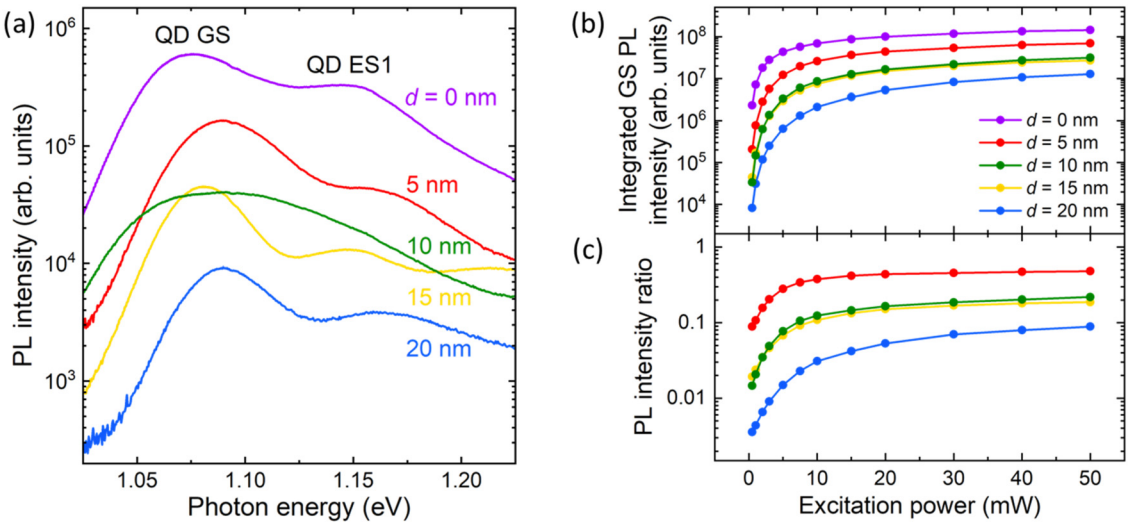

FIG. 2. (a) QD PL spectra measured at RT with an excitation power of 5 mW. (b) Integrated PL intensity of QD GS as a function of excitation power. (c) PL intensity ratio between $d = 5$, 10, 15, and 20 nm samples and $d = 0$ nm sample as a function of excitation power.

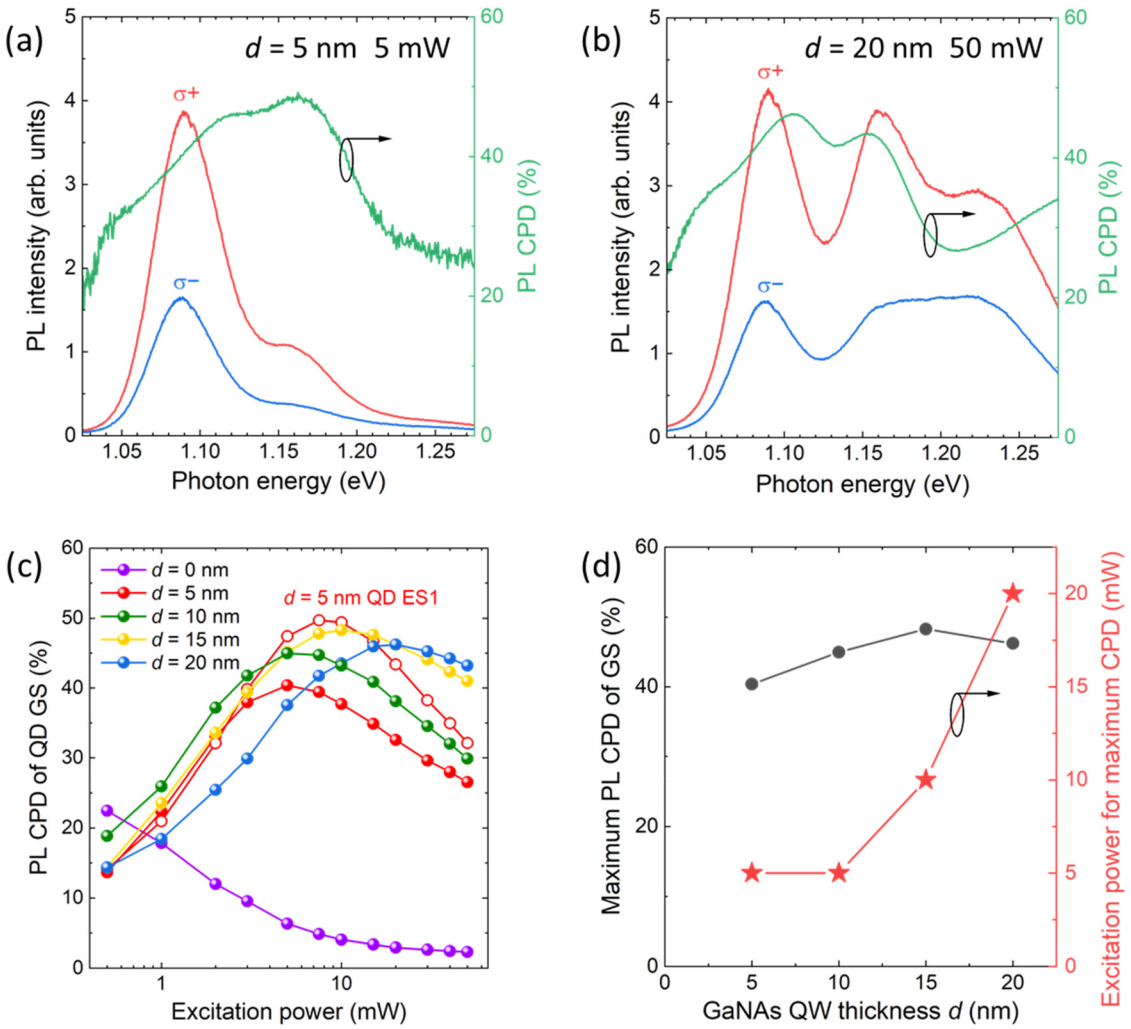

FIG. 3. Circularly polarized RT PL spectra and corresponding CPD of (a) $d = 5$ nm sample with an excitation power of 5 mW and (b) $d = 20$ nm sample with an excitation power of 50 mW. (c) PL CPD of QD GS as a function of excitation power. (d) Maximum PL CPD of QD GS and excitation power for maximum CPD as a function of GaNAs thickness.

GaNAs. Accordingly, the excitation power required for the maximum CPD decreased from 20 mW for the $d = 20$ nm sample to 5 mW for the $d = 5$ nm sample [Fig. 3(d)]. The maximum PL intensity, maximum PL CPD, and excitation power required for the maximum CPD are summarized in Table I. Here, the QD GS was chosen as an analyzed energy region, and the maximum PL intensity was normalized to the data of $d = 20$ nm sample. This result clearly shows that strong QD luminescence and high CPD at a lower excitation power can be achieved by reducing the GaNAs thickness. Conversely, the maximum CPD decreased from 48% for the $d = 15$ nm sample to 40% for the $d = 5$ nm sample. The slight decrease in the CPD can be attributed to the energy alignment between QW and QD. For the $d = 5$ nm sample, a higher electron energy of the QW GS was anticipated compared with that of the QD GS.[19] Therefore, the spin filtering of the GaNAs should significantly contribute to the PL of the QD ES.[18] Notably, a maximum CPD of 50% was achieved at QD ES1 in the $d = 5$ nm sample [Fig. 3(c)]. This finding indicates that reducing the GaNAs thickness does not impact the maximum spin polarization of the QDs. The comparison of PL CPD properties between this work and GaNAs-related previous works is presented in the supplementary material.

TABLE I. Maximum PL intensity, maximum PL CPD, and required excitation power.

GaNAs thickness (nm)	Maximum PL intensity	Maximum PL CPD (%)	Excitation power (mW)
5	5.4	40	5
10	2.5	45	5
15	2.1	48	10
20	1	46	20

TABLE II. Capture coefficient of conduction-band electrons by the Ga interstitial defects, γ_e, density of the defects, N_c, and effective capture rate of conduction-band electrons, $\gamma_e N_c$, deduced from the coupled rate equation analysis presented in the supplementary material.

GaNAs thickness (nm)	γ_e(cm^3 ps^{-1})	N_c(cm^{-3})	$\gamma_e N_c$(ps^{-1})
5	4.7×10^{-16}	4.9×10^{14}	0.230
10	3.3×10^{-16}	6.4×10^{14}	0.211
15	3.6×10^{-16}	6.0×10^{14}	0.216
20	2.3×10^{-16}	8.5×10^{14}	0.196

Next, the effect of the GaNAs thickness on the density of Ga interstitial defects was investigated. According to the previous studies,[16,17,26] we estimated the defect density from the excitation power-dependent PL CPD profiles of GaNAs using the nonlinear coupled rate equation. The details of the rate equation and fitting results are presented in the supplementary material. Table II shows the capture coefficient of conduction-band electrons by the Ga interstitial defects, γ_e, density of the defects, N_c, and effective capture rate of conduction-band electrons, $\gamma_e N_c$, deduced from the rate equation analysis. N_c tended to decrease with reducing GaNAs thickness except for $d = 10$ nm sample. Interestingly, γ_e was larger with thinner GaNAs thickness, resulting in larger $\gamma_e N_c$. This result means that the efficient capture of conduction-band electron spins can be achieved even at a low defect density for $d = 5$ nm sample. The combination of low N_c and large γ_e produces large spin polarization amplification (high PL CPD) at low excitation powers. Further detailed investigations are needed to reveal the origin of low N_c and large γ_e.

The time evolutions of the PL CPD of the QD GS at 10 and 50 mW are shown in Figs. 4(a) and 4(b), respectively, for the $d = 20$ and 5 nm samples. The time-dependent CPD behavior was influenced by the GaNAs thickness and the excitation power. At 10 mW, the sample with $d = 20$ nm exhibited a faster CPD increase from approximately 30%–50% and a rapid CPD decay after enhancement, whereas the sample with $d = 5$ nm indicated a slower CPD increase and retention of the temporally enhanced CPD. At 50 mW, a significant suppression of the CPD decay after the CPD increased to 60% was observed for the $d = 20$ nm sample. Conversely, for the $d = 5$ nm sample, the CPD was almost 0% in the initial time region and gradually increased to 50%. Utilizing rate equation analysis considering the capture of QD electron spins by the GaNAs DSs provides a quantitative understanding of spin polarization amplification behaviors.[19]

The schematic of the rate equation model of the GaNAs QW-InAs QD tunnel-coupled structure is shown in Fig. 5(a), illustrating the spin-dependent capture of QD electrons by the DSs. The QD PL is defined as the sum of the PL derived from the carriers injected from the GaAs barrier and GaNAs QW. Therefore, the PL component includes the number of carriers in the GaAs barrier (GaNAs QW) N_b

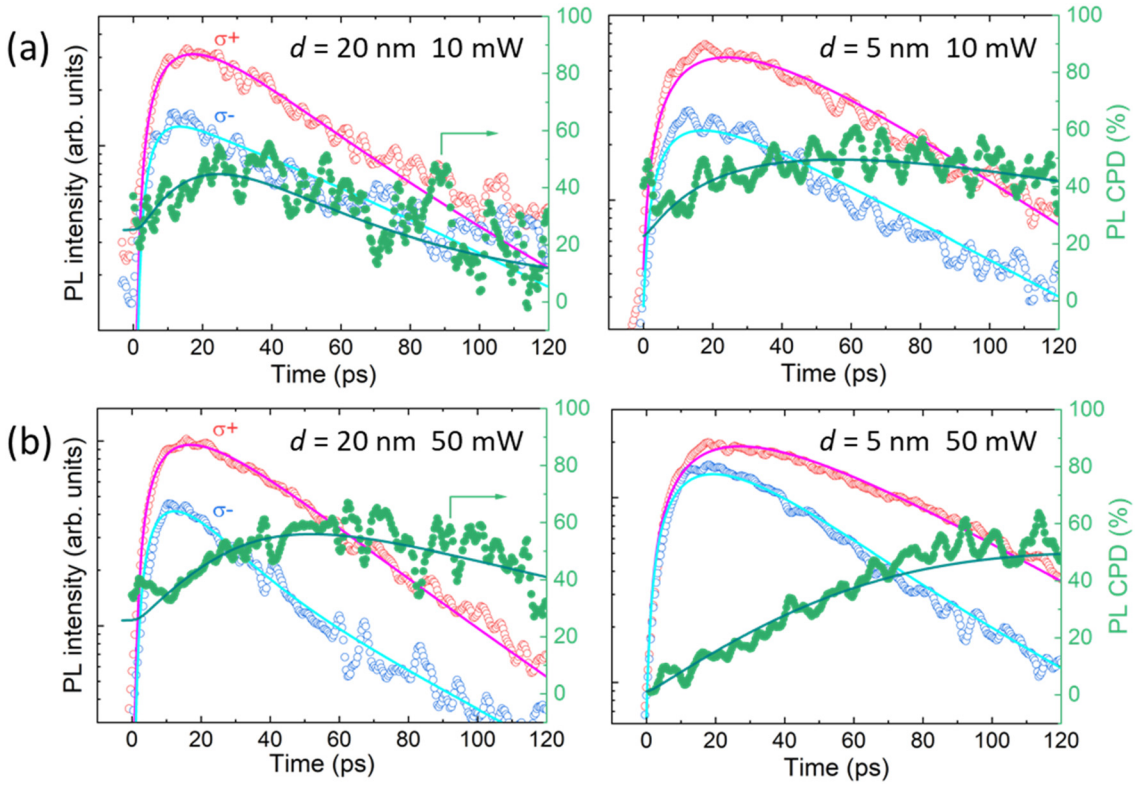

FIG. 4. Circularly polarized RT PL time profiles and corresponding CPDs of QD GS measured at (a) 10 mW and (b) 50 mW for the $d = 20$ nm sample (left) and $d = 5$ nm sample (right). The solid lines indicate the best-fitted results of the rate equation.

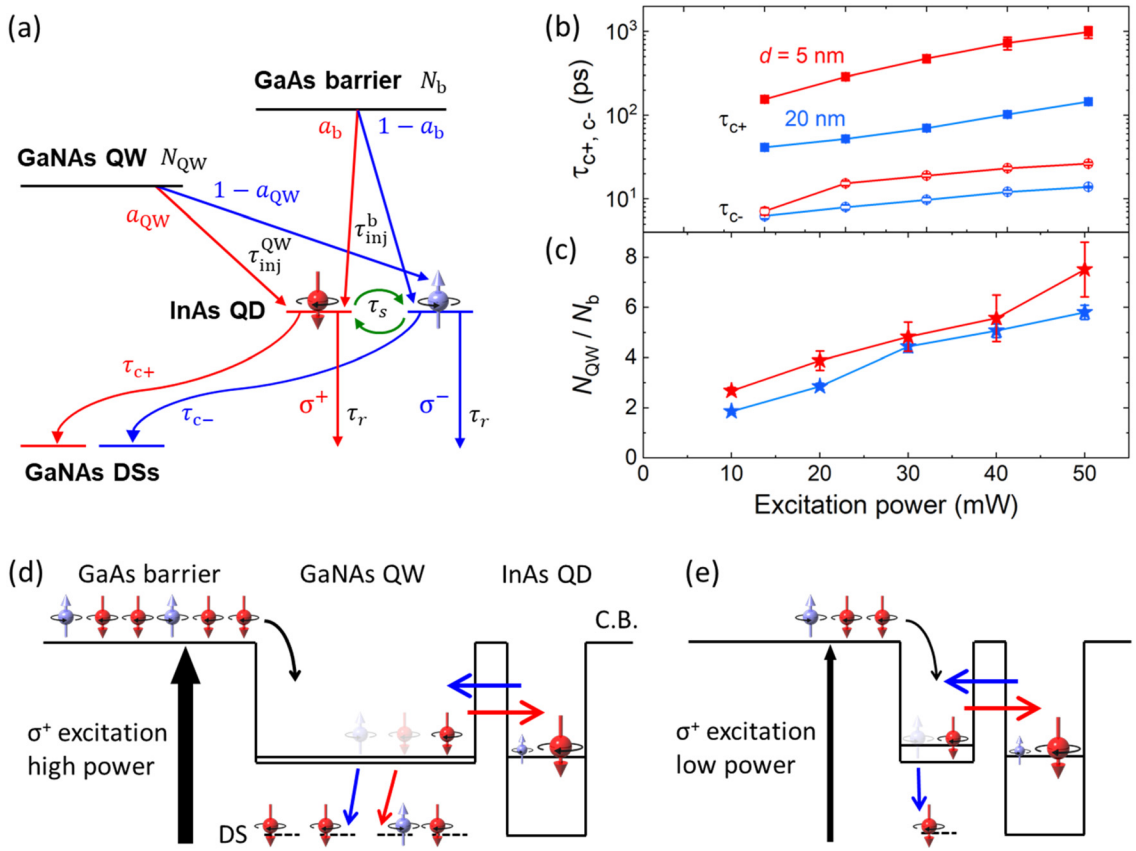

FIG. 5. (a) Rate equation model including the electron spin capture in the GaNAs DSs for the GaNAs QW-InAs QD tunnel-coupled structure. (b) $\tau_{c+,c-}$ and (c) N_{QW}/N_b as a function of excitation power for the $d = 5$ and 20 nm samples. Schematic of electron spin dynamics for (d) the $d = 20$ nm sample with a high excitation power and for (e) the $d = 5$ nm sample with a low excitation power.

(N_{QW}), along with the spin conservation factor during the injection process a_b (a_{QW}). Parameters τ_r, τ_s, and $\tau_{inj}^{b(QW)}$ denote the time constants for radiative recombination, spin relaxation, and spin injection from the GaAs barrier (GaNAs QW) to QDs, respectively. Notably, the time constant for the capture of QD majority (minority) spins by the DSs is defined as τ_{c+} (τ_{c-}). Further details of the rate equation are described elsewhere.[19] The best-fitted results of this rate equation for the time-dependent PL and CPD are shown in Figs. 4(a) and 4(b). The characteristic CPD amplification and PL decaying features were well expressed by optimizing the fitting parameters, $\tau_{c+,c-}$ and $N_{b,QW}$.

The excitation power dependence of $\tau_{c+,c-}$, as deduced from the rate equation fitting, is shown in Fig. 5(b). At 10 mW, τ_{c-} showed comparable results between the samples, whereas τ_{c+} was notably longer for the $d = 5$ nm sample. This outcome suggests that a smaller number of DSs and efficient capture of conduction-band electron spins discussed above can facilitate a spin-selective capture of QD electrons at a lower spin density. The resulting τ_{c+} significantly longer than τ_{c-} results in a retention of the temporally enhanced CPD [Fig. 4(a)]. In contrast, the larger number of DSs for $d = 20$ nm sample led to the capture of majority and minority spins from the QDs, resulting in a rapid CPD decay. τ_{c+} significantly increased relative to τ_{c-} as the excitation power increased. Consequently, τ_{c+} sufficiently longer than τ_{c-} was achieved at 50 mW even for the $d = 20$ nm sample. The imbalance of τ_{c+} and τ_{c-} is reflected in the significant suppression of CPD decay [Fig. 4(b)], similar to the time-dependent CPD at 10 mW for the $d = 5$ nm sample. The excitation power dependence of N_{QW}/N_b, as deduced from rate equation fitting, is shown in Fig. 5(c). N_{QW}/N_b was larger for the $d = 5$ nm sample than for the $d = 20$ nm sample, regardless of the excitation power, attributed to the smaller number of DSs. A gradual increase in N_{QW}/N_b with increasing excitation power was observed for both samples, attributed to the increased electron spin injection from the QW to QDs with the higher occupancy of DSs. As shown in Fig. 4(b), the sample with $d = 5$ nm demonstrated a low initial CPD at 50 mW, which then increased significantly with time. The weak QW-QD coupling for $d = 5$ nm sample resulted in slow electron spin injection from the QW to the QDs.[19] In this case, the initial CPD properties are predominantly characterized by the direct injection of depolarized electron spins from the GaAs barrier. This resulted in a state-filling effect in the QDs, reducing the CPD at high excitation powers [Fig. 3(c)]. Conversely, the combination of τ_{c+} significantly longer than τ_{c-} and large N_{QW}/N_b leads to the high CPD in the second-half time range.

Finally, we discuss the impact of GaNAs thickness on electron spin dynamics within the GaNAs-QD structure. As previously mentioned, the spin polarization amplification of QD electrons results from the spin-selective capture of QD electrons by spin-polarized DSs. Notably, the spin polarization of DSs is evident in the disparity between τ_{c+} and τ_{c-}. For the $d = 20$ nm sample, a substantial imbalance between τ_{c+} and τ_{c-} is achieved at higher excitation powers. This necessitates a high excitation spin density to optimize the spin-filtering effect, as shown in Fig. 5(d). Consequently, a high electron spin polarization of QDs is only achieved under high excitation powers [Fig. 3(c)]. In contrast, a significant imbalance between τ_{c+} and τ_{c-} is achieved at lower excitation powers for the $d = 5$ nm sample. This suggests that the spin-filtering effect can be maximized at a lower excitation spin density, resulting in a high electron spin polarization of QDs at low excitation powers [Fig. 5(e)].

In summary, we investigated the effects of the GaNAs thickness on the excitation power-dependent PL intensity and PL CPD of tunnel-coupled InAs QDs. When the GaNAs thickness decreased from 20 to 5 nm, the QD PL intensity significantly increased by over one order of magnitude at low excitation powers. The enhanced PL intensity was attributed to the reduced electron capture in the GaNAs DSs, originating from their limited number. Furthermore, the reduction in GaNAs thickness led to a decrease in the excitation power at which the PL CPD reached its peak while maintaining a near-maximum value. The efficient spin-amplified luminescence of QDs resulted from the spin-selective capture of QD electrons by the DSs achieved at a low excitation spin density because the small number of DSs can reduce the number of captured electron spins required to spin-polarize the DSs. These findings highlight the potential of reducing GaNAs thickness to achieve both strong QD luminescence and high circular polarization at low excitation spin densities. The implications of this study are valuable for the advancement of spin-polarized light-emitting devices that utilize the GaNAs spin-filtering effect.

See the supplementary material for comparison of PL CPD properties between this work and previous works, and nonlinear coupled rate equation analysis.

This work was financially supported by JSPS KAKENHI (Grant Nos. JP16H06359, JP20K20433, JP21H01356, JP21KK0068, JP23K26153, and JP24K00913), JST FOREST (Grant No. JPMJFR202E), JST ALCA-Next (Grant No. JPMJAN23E5), and NEDO (Grant No. P14004). A part of this work was conducted at Hokkaido University, supported by the "Nanotechnology Platform Program" of the Ministry of Education, Culture, Sports, Science, and Technology (MEXT), Japan (No. JPMXP09F20HK0010).

AUTHOR DECLARATIONS

Conflict of Interest

The authors have no conflicts to disclose.

Author Contributions

Satoshi Hiura: Conceptualization (equal); Data curation (supporting); Formal analysis (equal); Funding acquisition (equal); Methodology (equal); Project administration (lead); Supervision (lead); Writing – original draft (lead); Writing – review & editing (equal). **Shino Sato:** Conceptualization (supporting); Data curation (equal); Formal analysis (equal); Resources (lead); Writing – original draft (supporting); Writing – review & editing (supporting). **Shunsuke Sakano:** Data curation (equal); Formal analysis (equal); Writing – review & editing (supporting). **Junichi Takayama:** Formal analysis (supporting); Software (lead); Writing – review & editing (supporting). **Akihiro Murayama:** Conceptualization (equal); Funding acquisition (equal); Methodology (equal); Project administration (supporting); Supervision (supporting); Writing – review & editing (equal).

DATA AVAILABILITY

The data that support the findings of this study are available from the corresponding author upon reasonable request.

REFERENCES

[1]R. Jansen, Nat. Mater. **11**, 400 (2012).
[2]D. Khokhriakov, S. Sayed, A. M. Hoque, B. Karpiak, B. Zhao, S. Datta, and S. P. Dash, Phys. Rev. Appl. **18**, 064063 (2022).
[3]P. A. Dainone, N. F. Prestes, P. Renucci, A. Bouché, M. Morassi, X. Devaux, M. Lindemann, J.-M. George, H. Jaffrès, A. Lemaitre, B. Xu, M. Stoffel, T. Chen, L. Lombez, D. Lagarde, G. Cong, T. Ma, P. Pigeat, M. Vergnat, H. Rinnert, X. Marie, X. Han, S. Mangin, J.-C. Rojas-Sánchez, J.-P. Wang, M. C. Beard, N. C. Gerhardt, I. Žutić, and Y. Lu, Nature **627**, 783 (2024).
[4]D. Apalkov, A. Khvalkovskiy, S. Watts, V. Nikitin, X. Tang, D. Lottis, K. Moon, X. Luo, E. Chen, A. Ong, A. Driskill-Smith, and M. Krounbi, J. Emerging Technol. Comput. Syst. **9**, 1 (2013).
[5]X. Dong, X. Wu, G. Sun, Y. Xie, H. Li, and Y. Chen, in *Proceedings of the 45th Annual Design Automation Conference* (ACM, New York, NY, 2008), pp. 554–559.
[6]K. L. Wang, J. G. Alzate, and P. K. Amiri, J. Phys. D: Appl. Phys. **46**, 074003 (2013).
[7]F. Meier and B. Zakharchenya, *Optical Orientation* (Elsevier, North Holland, Amsterdam, 1984).
[8]T.-P. Hsieh, P.-C. Chiu, J.-I. Chyi, H.-S. Chang, W.-Y. Chen, T. M. Hsu, and W.-H. Chang, Appl. Phys. Lett. **89**, 053110 (2006).
[9]M. Sugawara and M. Usami, Nat. Photonics **3**, 30 (2009).
[10]A. V. Khaetskii and Y. V. Nazarov, Phys. Rev. B **61**, 12639 (2000).
[11]J. M. Elzerman, R. Hanson, L. H. Willems van Beveren, B. Witkamp, L. M. K. Vandersypen, and L. P. Kouwenhoven, Nature **430**, 431 (2004).
[12]M. Kroutvar, Y. Ducommun, D. Heiss, M. Bichler, D. Schuh, G. Abstreiter, and J. J. Finley, Nature **432**, 81 (2004).
[13]S. Sato, S. Hiura, J. Takayama, and A. Murayama, Appl. Phys. Lett. **116**, 182401 (2020).
[14]S. Hiura, M. Takishita, J. Takayama, S. Sato, and A. Murayama, Phys. Rev. Appl. **14**, 044011 (2020).
[15]D. Lagarde, L. Lombez, X. Marie, A. Balocchi, T. Amand, V. K. Kalevich, A. Shiryaev, E. Ivchenko, and A. Egorov, Phys. Status Solidi A **204**, 208 (2007).
[16]X. J. Wang, I. A. Buyanova, F. Zhao, D. Lagarde, A. Balocchi, X. Marie, C. W. Tu, J. C. Harmand, and W. M. Chen, Nat. Mater. **8**, 198 (2009).
[17]Y. Huang, V. Polojarvi, S. Hiura, P. Hojer, A. Aho, R. Isoaho, T. Hakkarainen, M. Guina, S. Sato, J. Takayama, A. Murayama, I. A. Buyanova, and W. M. Chen, Nat. Photonics **15**, 475 (2021).
[18]S. Park, S. Hiura, H. Kise, J. Takayama, K. Sueoka, and A. Murayama, Nanoscale **15**, 16784 (2023).
[19]S. Sato, S. Hiura, J. Takayama, and A. Murayama, Appl. Phys. Lett. **123**, 232405 (2023).
[20]K. Etou, S. Hiura, S. Park, J. Takayama, A. Subagyo, K. Sueoka, and A. Murayama, Phys. Rev. Appl. **19**, 024055 (2023).

[21]T. Kiba, X. Yang, T. Yamamura, Y. Kuno, A. Subagyo, K. Sueoka, and A. Murayama, Appl. Phys. Lett. **103**, 082405 (2013).
[22]T. Yamamura, T. Kiba, X. Yang, J. Takayama, A. Subagyo, K. Sueoka, and A. Murayama, J. Appl. Phys. **116**, 094309 (2014).
[23]S. Hiura, K. Takeishi, M. Urabe, K. Itabashi, J. Takayama, T. Kiba, K. Sueoka, and A. Murayama, Appl. Phys. Lett. **113**, 023104 (2018).
[24]S. Hiura, S. Saito, J. Takayama, T. Kiba, and A. Murayama, Appl. Phys. Lett. **115**, 013102 (2019).
[25]F. Zhao, A. Balocchi, G. Truong, T. Amand, X. Marie, X. J. Wang, I. A. Buyanova, W. M. Chen, and J. C. Harmand, J. Phys: Condens. Matter **21**, 174211 (2009).
[26]S. Chen, Y. Huang, D. Visser, S. Anand, I. A. Buyanova, and W. M. Chen, Nat. Commun. **9**, 3575 (2018).